

# Surface Wetting of Liquid Nanodroplets: Droplet Size Effects

David R. Heine, Gary S. Grest, Edmund B. Webb III

*Sandia National Laboratories, Albuquerque, New Mexico 87185*

(Dated: 23rd May 2019)

## Abstract

The spreading of liquid nanodroplets of different initial radii  $R_0$  is studied using molecular dynamics simulation. Results for two systems, Pb on Cu(111) and a coarse grained polymer model are presented for Pb droplets ranging in size from  $\sim 55\,000$  to  $220\,000$  atoms and polymer droplets ranging in size from  $\sim 200\,000$  to  $780\,000$  monomers. In both cases, a precursor foot precedes the spreading of the main droplet. This precursor foot spreads diffusively,  $r_f^2(t) = 2D_{eff}t$  with an effective diffusion constant that exhibits a droplet size dependence  $D_{eff} \sim R_0^{1/2}$ . The radius of the main droplet  $r_b(t) \sim R_0^{4/5}$  in agreement with kinetic models for the cylindrical geometry studied.

Numerous practical problems are determined by the wetting of surfaces by liquids including adhesion, lubrication, coatings, plant protection, and oil recovery. The spreading of a droplet on a surface proceeds as the droplet balances the interfacial tensions between the solid, liquid, and vapor phases. Completely wetting droplets are known to form a monolayer film or precursor foot on the surface that spreads ahead of the droplet. For “high-energy” surfaces, spreading includes the formation of molecule-sized terraces along with the precursor foot [1, 2].

Although the spreading behavior of droplets on surfaces has been extensively studied, droplet size effects on the spreading dynamics are often ignored. These size effects can have a large influence on the wetting behavior, particularly when using nanoscale droplets such as in MEMS and microfluidic devices. For these devices, droplet size can strongly affect both the manufacturing speed, such as in microcontact printing, and the device performance.

The size dependence of the rate of change of the bulk droplet radius is well known and is present in models of droplet spreading. The molecular kinetic theory of liquids was developed by Eyring et al. [3] and applied to droplet spreading by Blake and Haynes [4]. In this model, the contact radius  $r_b(t)$  of the bulk region of the droplet scales with the droplet volume according to  $r_b(t) \sim R_0^{6/7}$  at late times for spherical droplets [5] and  $r_b(t) \sim R_0^{4/5}$  for cylindrical droplets [6]. The hydrodynamic model [7, 8] is based upon the solution of the equations of motion and continuity for the droplet. For the hydrodynamic model, the contact radius of the bulk region scales according to  $r_b(t) \sim R_0^{9/10}$  at late times for spherical droplets [5] and  $r_b(t) \sim R_0^{6/7}$  for cylindrical droplets [6]. The combined model is obtained by including the energy dissipation mechanisms from both the kinetic and hydrodynamic models [5]. For a cylindrical droplet, the combined spreading model was recently derived as [6]

$$\frac{dr_b(t)}{dt} = \frac{\gamma}{\frac{\zeta_0}{2} + \frac{2\eta(r_b(t)-a)\sin^2\theta}{r_b(t)(\theta-\sin\theta\cos\theta)}} \left( \frac{\theta}{\sin\theta} - \frac{\theta_0}{\sin\theta_0} \right), \quad (1)$$

$$\frac{d\theta}{dt} = \left( \frac{\theta - \sin\theta\cos\theta}{A} \right)^{1/2} \left( \cos\theta - \frac{\sin^3\theta}{\theta - \sin\theta\cos\theta} \right)^{-1} \frac{dr_b(t)}{dt}. \quad (2)$$

where the cross-sectional area  $A \sim R_0^2$ ,  $\gamma$  is the liquid/vapor surface tension,  $\zeta_0$  is the friction coefficient,  $\eta$  is the bulk fluid viscosity,  $a$  is the hydrodynamic cutoff, and  $\theta_0$  is the equilibrium contact angle. The kinetic and hydrodynamic models are obtained from Eq. 1

by setting  $\eta$  and  $\zeta_0$  to zero, respectively.

Experiments [9, 10] and simulation [6, 11, 12, 14] have shown that droplets often spread with a precursor foot preceding the main drop. This foot grows diffusively, though to the best of our knowledge there are no predictions for the dependence on the droplet size.

Molecular dynamics (MD) simulations allow us to measure the droplet size effects using either perfectly smooth or intentionally rough surfaces. This allows us to distinguish between phenomena such as the theoretical expression for the line tension presented as a correction to Young’s equation and the line tension presented as a one-dimensional surface tension. Here, we focus on the dynamics of spreading droplets. Although droplet size effects are often ignored when studying spreading dynamics, we show that both the surface diffusion rate in the precursor foot and the bulk spreading rate change with droplet size.

Here, we present MD simulations for two very different systems, a coarse-grained model of polymer nanodroplets and an explicit atom model of Pb on Cu(111), to study the dependence of the spreading rate of both the droplet and the precursor foot on the initial radius  $R_0$  of the droplet. Our results demonstrate that the observed behavior is a general phenomenon and does not depend on the system specifics. In both cases, the vapor pressure is low so that spreading does not occur via vaporization and condensation.

For polymer chains, the polymer is represented by spherical beads of mass  $m$  attached by springs, which interact with a truncated Lennard-Jones (LJ) potential,

$$U_{LJ}(r) = \begin{cases} 4\varepsilon \left[ \left(\frac{\sigma}{r}\right)^{12} - \left(\frac{\sigma}{r}\right)^6 \right] & r \leq r_c \\ 0 & r > r_c \end{cases} \quad (3)$$

where  $\varepsilon$  and  $\sigma$  are the LJ units of energy and length and the cutoff  $r_c = 2.5\sigma$ . The monomer-monomer interaction  $\varepsilon$  is used as the reference and all monomers have the same diameter  $\sigma$ . For bonded monomers, we apply an additional potential where each bond is described by the finite extensible nonlinear elastic (FENE) potential [13] with  $k = 30 \varepsilon/\sigma^2$  and  $R_0 = 1.5 \sigma$ . The substrate is modeled as a flat surface since it was found previously [14] that with the proper choice of thermostat, the simulations using a flat surface exhibit the same behavior as a realistic atomic substrate. Simulating a realistic substrate requires several times the total number of atoms in the simulation, thus using the flat surface greatly improves the computational efficiency. The interactions between the surface and the monomers in the droplet at a distance  $z$  from the surface are modeled using an integrated LJ potential with

the cutoff set to  $z_c = 2.2\sigma$  [14]. Here we present results for  $\varepsilon_w = 2.0\varepsilon$  which for  $N = 10$  is above the wetting transition  $\varepsilon_w^c = 1.75\varepsilon$ .

We apply the Langevin thermostat to provide a realistic representation of the transfer of energy in the polymer droplet. The Langevin thermostat simulates a heat bath by adding Gaussian white noise and friction terms to the equation of motion,

$$m_i \frac{d^2 \mathbf{r}_i}{dt^2} = -\Delta U_i - m_i \gamma_L \frac{d\mathbf{r}_i}{dt} + \mathbf{W}_i(t), \quad (4)$$

where  $m_i$  is the mass of monomer  $i$ ,  $\gamma_L$  is the friction parameter for the Langevin thermostat,  $-\Delta U_i$  is the force acting on monomer  $i$  due to the potentials defined above, and  $\mathbf{W}_i(t)$  is a Gaussian white noise term. Coupling all of the monomers to the Langevin thermostat would have the unphysical effect of screening the hydrodynamic interactions in the droplet and not damping the monomers near the surface stronger than those in the bulk. To overcome this, we use a Langevin coupling term with a damping rate that decreases exponentially away from the substrate [15]. We choose the form  $\gamma_L(z) = \gamma_L^s \exp(\sigma - z)$  where  $\gamma_L^s$  is the surface Langevin coupling and  $z$  is the distance from the substrate. In this paper, we present results for  $\gamma_L^s = 3.0$  and  $10.0 \tau^{-1}$ . The larger  $\gamma_L^s$  corresponds to an atomistic substrate with large corrugation and hence large dissipation and slower diffusion near the substrate.

For Pb on Cu(111), interactions are described via embedded atom method (EAM) interatomic potentials wherein the energy for  $N$  atoms is [16]

$$E = \sum_{i=1}^N [F_i(\rho_i) + \frac{1}{2} \sum_{j \neq i} \phi_{ij}(r)]. \quad (5)$$

In Eq. 5,  $\rho_i$  is the electron density at atom  $i$ ,  $\rho_i = \sum_{j \neq i} \rho_j^a(r)$ , where  $\rho_j^a(r)$  is the spherically symmetric electron density contributed by atom  $j$ , a distance  $r$  from  $i$ .  $F_i(\rho_i)$  is the energy associated with embedding atom  $i$  into an electron density  $\rho_i$  and  $\phi_{ij}(r)$  is a pair potential between atoms  $i$  and  $j$ . The many-body nature of  $F_i(\rho_i)$  in Eq. 5 makes the EAM superior to pair potentials for describing bonding in metal systems. The interactions for Cu, Pb, and the cross-term between them were previously parameterized [17, 18, 19]. The Cu(111) substrate was described via an explicit atom description with dimension in the surface normal direction equal to four times the potential cutoff  $r_c = 5.5 \text{ \AA}$ . The substrate was equilibrated at the proper lattice constant prior to joining with the drop. Atoms in the  $2r_c$  planes furthest from the surface are held rigid and the rest are permitted to relax according to MD equations of

motion throughout all simulations. Because the substrate is represented atomistically for Pb(l) on Cu(111), we thermostat only atoms in the substrate using a Nose-Hoover thermostat algorithm.

All of the droplets presented here are modeled as hemicylinders as described previously [6]. The system is periodic in the y direction with length  $L_y$  and open in the other two directions. This allows a larger droplet radius to be studied using the same number of monomers than in the spherical geometry. Polymeric droplets have initial droplet radii of  $R_0 \cong 50, 80, \text{ and } 120 \sigma$ , cross-sectional areas  $A \cong 2690, 7490, \text{ and } 18\,200 \sigma^2$  and a total size  $N \cong 200\,000, 350\,000, \text{ and } 780\,000$  monomers, respectively, with  $L_y = 60 \sigma$  for  $R_0 \cong 50 \sigma$  and  $L_y = 40 \sigma$  for  $R_0 \geq 80 \sigma$ . Pb(l) droplets are studied with  $R_0 \cong 20, 30, \text{ and } 40 \text{ nm}$ ,  $A \cong 630, 1400, \text{ and } 2500 \text{ nm}^2$  and  $N \cong 55\,000, 122\,000, \text{ and } 220\,000$  atoms in the drop, respectively, with  $L_y = 27 \text{ \AA}$ . The substrates for the three drop sizes in the Pb(l) on Cu(111) systems contained  $N \cong 85\,000, 128\,000, \text{ and } 170\,000$  Cu atoms.

The equations of motion are integrated using a velocity-Verlet algorithm. For polymer spreading, we use a time step of  $\Delta t = 0.01 \tau$  where  $\tau = \sigma \left(\frac{m}{\varepsilon}\right)^{1/2}$ . The simulations are performed at a temperature  $T = \varepsilon/k_B$  using the LAMMPS code [24]. For Pb(l) on Cu(111),  $\Delta t = 1 \text{ fs}$ ,  $T = 700 \text{ K}$ , and the code PARADYN [25] was used.

For the polymeric system, it was shown previously [14] by measuring the equilibrium contact angle that finite system size effects become negligible for droplets containing 50 000 monomers or more. Here, we study the size dependence of the spreading behavior for droplets substantially larger than this finite size limit by using a minimum droplet size of 200 000 monomers in order to simultaneously study the bulk and precursor foot regions. This is shown in Fig. 1 which shows the foot extending beyond the bulk region. For the monomeric liquid system Pb on Cu(111), computational requirements for modeling the substrate are more significant so we use a minimum drop size  $N \sim 55\,000$  atoms. In a prior work [20], wetting of Pb(l) drops on Cu(100) and Cu(111) was simulated using this model. For Pb(l) on Cu(111), a precursor film rapidly advanced ahead of the main drop in a diffusive manner (see Fig. 1); furthermore, the drop reached an equilibrium but finite contact angle  $\theta_0 = 33^\circ$  on top of the prewetting film. These results are in excellent agreement with experiment [20, 21, 22, 23]. This system exhibits negligible exchange of atoms between the liquid and solid, permitting evaluation of system size effects for non-reactive wetting in the case of a monomeric liquid with low vapor pressure.

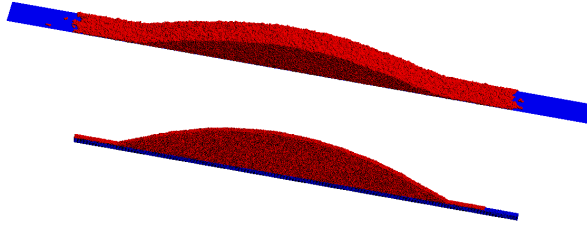


Figure 1: (color online) Cross-section snapshots from the simulations. A droplet composed of chain length  $N = 10$  polymers with initial radius  $R_0 = 80 \sigma$ ,  $\varepsilon_w = 2.0 \varepsilon$ , and  $\gamma_L^s = 3.0 \tau^{-1}$  at  $t = 71\,600 \tau$  (top). A Pb(l) droplet with  $R_0 = 40 \text{ nm}$  on Cu(111) at  $t = 3.6 \text{ ns}$  (bottom).

For the simulations presented here, we extract the instantaneous contact radius  $r_b(t)$  and contact angle  $\theta(t)$  every  $400 \tau$  for the polymer system and every  $4 \text{ ps}$  for the metal system according to the procedure described previously [6, 20]. The scaling predictions of the kinetic and hydrodynamic models are applied to the bulk contact radius data for  $\varepsilon_w = 2.0 \varepsilon$  and  $\gamma_L^s = 3.0$  and  $10.0 \tau^{-1}$  in Fig. 2a where dividing the bulk contact radius by  $R_0^{4/5}$  for each of three droplet sizes causes the data to collapse to a single curve. The  $R_0^{6/7}$  scaling of the same data, shown in Fig. 2b, does not fit as well because hydrodynamic energy dissipation has only a weak influence on the spreading rate for the conditions used in these simulations [6]. Similar results are found for Pb on Cu(111) (see Figs. 3a and b) because here we also have a low viscosity, rapidly spreading droplet.

Previous simulations of polymer droplet spreading [6] have shown that the hydrodynamic model, Eqs. 1 and 2 with  $\zeta_0 = 0$ , adequately fits the data only for the higher viscosity (longer chains) and slower spreading droplets. Here, a consistent improvement of the fit to the hydrodynamic model is observed for the three droplet sizes in going from the faster  $\gamma_L^s = 3.0 \tau^{-1}$  to the slower  $\gamma_L^s = 10.0 \tau^{-1}$  conditions as well as going from smaller to larger droplets. Both the kinetic and combined models fit the data well for all of the droplets although the combined model tends to produce less reasonable values of the fitting parameters [14].

It is difficult to study the precursor foot dynamics experimentally due to factors such as the surface roughness and contact line pinning. The dynamics are known to be diffusive with a spreading rate proportional to  $t^{1/2}$ . Joanny and de Gennes predicted the height profile of the precursor foot to be proportional to  $1/r$  [9, 26], but models relating the precursor foot dynamics to the droplet dimensions, such as those presented above for the bulk dynamics,

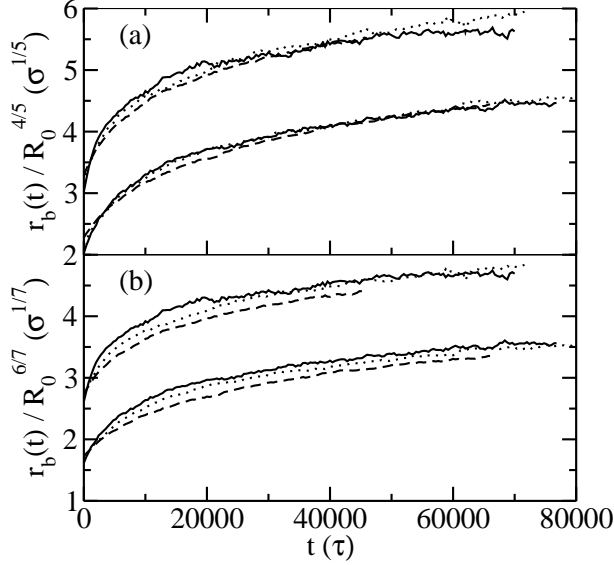


Figure 2: Scaling of the bulk contact radius for three droplet sizes based on the initial radii  $R_0 = 50\sigma$  (solid line),  $R_0 = 80\sigma$  (dotted line), and  $R_0 = 120\sigma$  (dashed line) using the predictions of (a) the kinetic model and (b) the hydrodynamic model. Each droplet is composed of chain length  $N = 10$  polymers with  $\varepsilon_w = 2.0\varepsilon$ ,  $\gamma_L^s = 3.0$  (upper curves) and  $10.0\tau^{-1}$  (lower curves). The  $\gamma_L^s = 3.0\tau^{-1}$  curves are shifted upward for clarity.

are not available. Like the figures of the bulk contact radius, the size dependence is evident in the precursor foot contact radius as well. This is shown in Fig. 4 where the precursor foot contact radius is divided by the initial contact radius raised to the power  $n$  where  $n = 1/2$ . For the  $\gamma_L^s = 10.0\tau^{-1}$  system, the curves in Fig. 4a show the same asymptotic behavior, but differences in the initial contact radius cause the curves to be offset by a constant value at later times. For the  $\gamma_L^s = 3.0\tau^{-1}$  system, Fig. 4a shows the offset is less severe and the curves for the three different droplet sizes overlap. For Pb(l) on Cu(111), Fig. 4b shows results in this system are quite similar to what is seen for the  $\gamma_L^s = 3.0\tau^{-1}$  case in the polymeric systems. This implies that Pb(l) on Cu(111) corresponds to a lower surface corrugation which, given the significant lattice mismatch between Pb and Cu and the high density packing of the (111) surface, is a reasonable result.

For diffusive spreading in two dimensions, the precursor foot contact radius follows  $r_f^2(t) = 2D_{eff}t$  where  $D_{eff}$  is the effective diffusion coefficient. Within the uncertainty of our data, these results are consistent with  $D_{eff} \sim R_0^{1/2}$  even though the polymeric sys-

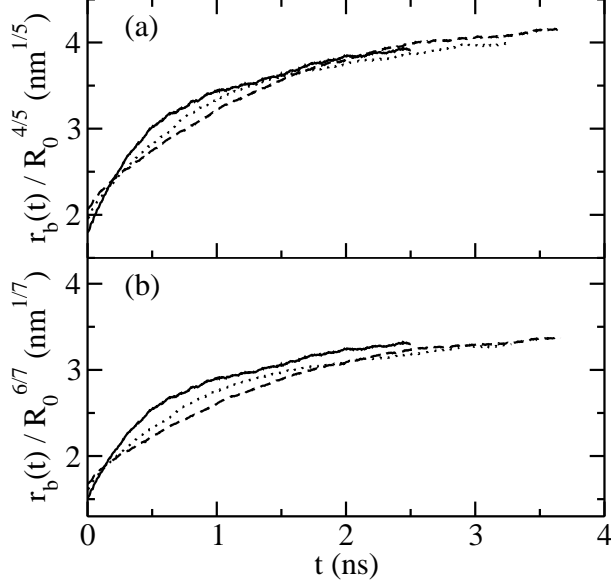


Figure 3: Scaling of the bulk contact radius of three Pb(l) droplet sizes based on the initial radii  $R_0 = 20 \text{ nm}$  (solid line),  $R_0 = 30 \text{ nm}$  (dotted line), and  $R_0 = 40 \text{ nm}$  (dashed line) using the predictions of (a) the kinetic model and (b) the hydrodynamic model.

tems are completely wetting and the metal system is nonwetting. For the  $\gamma_L^s = 10.0 \tau^{-1}$  system,  $D_{eff} \sim R_0^{0.65}$  collapses the data onto a master curve better than  $R_0^{1/2}$ . This may be due to the fact that the high coupling constant reduces the foot spreading rate to that of the bulk droplet, so the  $D_{eff} \sim R_0^{1/2}$  scaling is not valid when the spreading of the bulk droplet interferes with the precursor foot diffusion. At present, there is no theoretical model we are aware of which predicts the dependence of  $D_{eff}$  on  $R_0$ .

In summary, we study the droplet size dependence of polymer nanodroplets spreading in cylindrical geometries using molecular dynamics simulation. Our results follow the kinetic model of droplet spreading, which predicts a  $R_0^{4/5}$  size scaling of the bulk droplet contact radius. Theories describing the dynamics of the precursor foot do not predict a droplet size dependence. The spreading rate of the precursor foot is known to be diffusive, but here we show that the effective diffusion coefficient has a droplet size dependence,  $D_{eff} \sim R_0^{1/2}$ , which can be utilized in the design of surface wetting applications. For Pb(l) on Cu(111), use of a realistic interatomic potential results in non-reactive wetting (in agreement with experiment). Furthermore, vapor pressure is low despite this being a monomeric liquid. As such, spreading mechanisms for the metal systems are similar to the polymeric systems

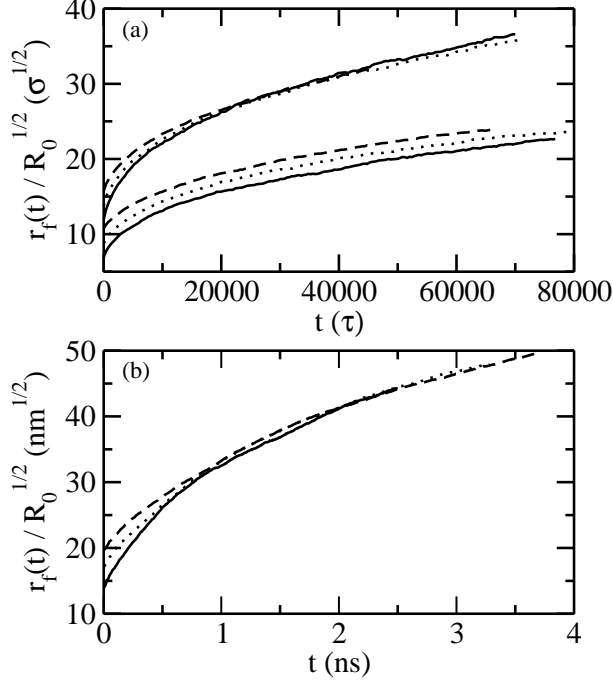


Figure 4: (a) Polymeric systems precursor foot spreading rate divided by  $R_0^{1/2}$  for  $R_0 = 50 \sigma$  (solid line),  $R_0 = 80 \sigma$  (dotted line), and  $R_0 = 120 \sigma$  (dashed line) for  $\varepsilon_w = 2.0 \varepsilon$  and  $\gamma_L^s = 10.0 \tau^{-1}$  (lower curves) and for  $\gamma_L^s = 3.0 \tau^{-1}$  (upper curves). Each droplet is composed of chain length  $N = 10$  polymers. The  $\gamma_L^s = 3.0 \tau^{-1}$  curves have been shifted upward for clarity. (b) Precursor foot spreading rate for Pb(l) on Cu(111) divided by  $R_0^{1/2}$  for  $R_0 = 20, 30,$  and  $40 \text{ nm}$  at  $T = 700 \text{ K}$ .

studied and the same size dependence of the spreading rate is found despite the fact that these are two very different systems.

Sandia is a multiprogram laboratory operated by Sandia Corporation, a Lockheed Martin Company, for the United States Department of Energy's National Nuclear Security Administration under Contract No. DE-AC04-94AL85000.

---

[1] F. Heslot, A. M. Cazabat, and P. Levinson, *Phys. Rev. Lett.* **62**, 1286 (1989).  
[2] F. Heslot, A. M. Cazabat, P. Levinson, and N. Fraysse, *Phys. Rev. Lett.* **65**, 599 (1990).  
[3] S. Gladstone, K. J. Laidler, and H. J. Eyring, *The Theory of Rate Processes* (McGraw-Hill, New York, 1941).  
[4] T. D. Blake and J. M. Haynes, *J. Coll. Interface Sci.* **30**, 421 (1969).

- [5] M. J. de Ruijter, J. De Coninck, and G. Oshanin, *Langmuir* **15**, 2209 (1999).
- [6] D. R. Heine, G. S. Grest, and E. B. Webb III, *Phys. Rev. E* **70**, 011606 (2004).
- [7] R. G. Cox, *J. Fluid Mech.* **168**, 169 (1986).
- [8] A. E. Seaver and J. G. Berg, *J. App. Poly. Sci.* **52**, 431 (1994).
- [9] P. G. de Gennes, *Rev. Mod. Phys.* **57**, 827 (1985).
- [10] F. Heslot, N. Fraysse, and A. M. Cazabat, *Nature* **338**, 640 (1989).
- [11] J. A. Nieminen, D. B. Abraham, M. Karttunen, and K. Kaski, *Phys. Rev. Lett.* **69**, 124 (1992).
- [12] S. Bekink, S. Karaborni, G. Verbist, and K. Esselink, *Phys. Rev. Lett.* **76**, 3766 (1996).
- [13] K. Kremer and G. S. Grest, *J. Chem. Phys.* **92**, 5057 (1990).
- [14] D. R. Heine, G. S. Grest, and E. B. Webb III, *Phys. Rev. E* **68**, 061603 (2003).
- [15] O. M. Braun and M. Peyrard, *Phys. Rev. E* **63**, 046110 (2001).
- [16] M. S. Daw and M. I. Baskes, *Phys. Rev. B* **29**, 6443 (1984).
- [17] S. M. Foiles, M. I. Baskes, and M. S. Daw, *Phys. Rev. B* **33**, 7983 (1986).
- [18] H. S. Lim, C. K. Ong, and F. Ercolessi, *Surf. Sci.* **269/270**, 1109 (1992).
- [19] J. J. Hoyt, J. W. Garvin, E. B. Webb III, and M. Asta, *Modelling Simul. Mater. Sci. Eng.* **11**, 287 (2003).
- [20] E. B. Webb III, G. S. Grest, and D. R. Heine, *Phys. Rev. Lett.* **91**, 236102 (2003).
- [21] G. L. J. Bailey and H. C. Watkins, *Proc. Phys. Soc. London B* **63**, 350 (1950).
- [22] G. Prévot, C. Cohen, J. M. Guigner, and D. Schmaus, *Phys. Rev. B* **61**, 10393 (2000).
- [23] J. Moon, J. Lowekamp, P. Wybblatt, S. Garoff, and R. M. Suter, *Surf. Sci.* **488**, 73 (2001).
- [24] S. Plimpton, *J. Comput. Phys.* **117**, 1 (1995).
- [25] S. J. Plimpton and B. A. Hendrickson, *Mat. Res. Soc. Proc.* **291**, 37 (1993).
- [26] J. F. Joanny, *Thesis, Université Paris VI* (1985).